Magneto-Plasmonics-Enhanced Colorimetric Lateral Flow Immunoassay Using Magnetic-Gold Nanostars

Supriya Atta, [a, b] *Taylor L. Thorsen,*[a, c] *Yuanhao Zhao,* [a, b] *Sebastian Sanchez,*[c] *Haydon J. Hill,*[d] *Vanessa K. Berner,*[d] *Marcellene A. Gates-Hollingsworth,*[d] *Jasmine Pramila Devadhasan,*[e] *Alexander Jarrett Summers,*[e] *Jian Gu,*[e,f] *Douglas C. Montgomery,*[e,g] *David P. AuCoin,*[d] *Frederic Zenhausern ,*[e,f] *Tuan Vo-Dinh* [a, b, c(*)]

[a] Fitzpatrick Institute for Photonics, [b] Department of Biomedical Engineering, [c] Department of Chemistry, Duke University, Durham, NC 27708, USA

[d] Department of Microbiology and Immunology, University of Nevada, Reno School of Medicine, Reno, NV 89557, USA

[e] Center for Applied Nano Bioscience and Medicine, College of Medicine, University of Arizona, Phoenix, AZ 85004, USA

[f] Department of Basic Medical Sciences; The University of Arizona, College of Medicine, 475 N 5th St., Phoenix, AZ 85004, USA

[g] School of Computing and Augmented Intelligence, Ira A. Fulton Schools of Engineering Arizona State University, Tempe AZ 85281, USA

(*) Corresponding Author: tuan.vodinh@duke.edu

KEYWORDS. nanostar, magnetic, LFIA, sensing, colorimetric.

Abstract

Colorimetric lateral flow immunoassays (LFIA) have revolutionized point-of-care testing (POCT) methods by providing simple, rapid, accessible, and instrumentation-free detection of infectious diseases. However, conventional LFIAs relying on gold nanospheres (GNPs) can suffer from limited sensitivity due to weak colorimetric signal intensity at the test line, restricting their diagnostic potential. To overcome this limitation, we developed a magneto-plasmonics enhanced colorimetric LFIA (mpLFIA)- a breakthrough platform that integrates a novel hybrid nanoparticle system-magnetic gold nanostars (mpGNS). By leveraging dual enhancement mechanisms - magnetic preconcentration and plasmonic amplification through the gold nanostar shell coating of the magnetic core- the mpLFIA achieves unprecedented signal intensity and detection performance. Among the tested mpGNS variants, mpGNS-3- distinguished by its longest spikes and highest branch density- emerged as the most effective colorimetric signal amplifier when evaluated using Rift Valley fever virus (RVFV) nucleoprotein as a model analyte. Our mpLFIA platform achieves an outstanding limit of detection (LOD) of 2.24 pg/mL for RVFV nucleoprotein in 1X PBS buffer, demonstrating a 1000-fold enhancement over conventional GNP-based assays. Our prototype mpLFIA platform, utilizing highly spiked mpGNS-3, exhibits great potential as a powerful bioanalytical tool, combining high sensitivity with practical portability for point-of-care applications.

Introduction

The colorimetric lateral flow immunoassay (LFIA) is remarkable detection platform that has greatly accelerated the growth of point-of-care testing (POCT) by providing a simple, affordable, and portable solution that operates without the need for any instrumentation[1, 2]. Unlike other POCT techniques such as lab-on-a-chip devices[3], bench-top analyzers[4], microfluidic devices[5]-which often involve complex microfluidics and sophisticated optical readouts[6],

colorimetric LFIAs stand out for their streamlined design and ease of use. More importantly, colorimetric LFIAs are paper based, with rapid visual results determined through the appearance of a line upon the introduction of a "positive" sample. The traditional colorimetric LFIA assay typically employs gold nanospheres due to their simple synthesis and distinct red color, which is readily visible on the test line[7-9]. This intense red color contrast allows for easy detection, enabling quick interpretation of either positive or negative results. However, despite the simplicity of traditional gold nanosphere-based platforms, colorimetric LFIAs often suffer from limited sensitivity, increasing the risk of misdiagnosis due to false negatives[10-13]. This limitation is primarily attributed to the inadequate optical brightness of gold nanospheres, which affects the visibility and accuracy of the test results.

To address this drawback in colorimetric LFIA sensitivity, additional readout methods have been explored to better improve confidence in diagnosis[14]. Coupling colorimetric detection with a quantitative technique will allow the analyte to be detected at lower concentrations within earlier stages of infection or physical state. Other analytical techniques, such as fluorescence[15], photothermal[16], and surface-enhanced Raman scattering (SERS)[17, 18], offer enhanced sensitivity but are less suitable for POCT due to their reliance on additional instrumentation, which limits their portability and practicality in field settings[19-21]. Therefore, there is a significant demand for enhancing colorimetric LFIA by employing various types of nanoparticles. Several studies have explored different nanoparticle systems to improve the performance of colorimetric LFIA.

Effective nanoparticle systems for colorimetric LFIA include a variety of nanoparticle systems such as polymeric polydopamine nanoparticles (PDA)[22], metal oxide nanoparticles including iron oxide nanoparticles[23, 24], dye coated silica nanoparticles[25], platinum nanoparticles[26],

plasmonic noble metal nanoparticles such as gold[27] and silver[28] nanoparticles, and hybrid multi-metallic nanoparticle systems[29, 30]. Among these nanoparticle systems, plasmonically active nanoparticles show great promise for achieving enhanced colorimetric optical brightness. These materials exhibit bright optical properties, making them highly effective in colorimetric readout methods[31]. It is important to note that the color intensity of plasmonic nanoparticles is primarily governed by their localized surface plasmon resonance (LSPR) properties, which are linked to the extinction coefficient that dictates the overall color of the nanoparticle system[32]. The extinction coefficient is affected by the nanoparticle's size, shape, elemental composition, and surface modifications. For instance, anisotropic gold nanoparticles, such as nanocages, nanoshells, and nanostars, exhibit enhanced visual detection primarily due to their high extinction coefficient[33-35]. Out of different morphologies of gold nanoparticle systems, gold nanostars represent a more promising nanoplatform than other nanoparticle morphologies for enhancing the performance of colorimetric LFIA assays. This advantage primarily stems from the strong localized surface plasmon resonance (LSPR) of the nanostars, resulting in exceptionally high molar extinction coefficients, which further enhance their optical brightness in colorimetric LFIA assays[36-38]. Additionally, their larger surface area, characterized by a spherical core with multiple protruding spikes, significantly enhances antibody conjugation efficiency, thereby improving LFIA assay performance[39]. For example, our recent work demonstrated that sharp-spiked gold nanostars and bimetallic gold nanostars provide enhanced colorimetric sensitivity compared to conventional gold nanosphere-based colorimetric LFIA[40, 41]. Although anisotropic gold nanoparticles demonstrate promising colorimetric LFIA sensitivity, their detection limit remains in the ng/mL range. Therefore, further improvements are needed to enhance LFIA sensitivity for detecting ultra-low analyte concentrations.

Literature has explored incorporating secondary materials into the plasmonics gold nanoparticle system, with magnetic iron (III) oxide (Fe_3O_4) being a notable example. This addition not only enhances plasmonic properties[42, 43], but also enables magnetic-assisted nanoparticle concentration upon applying a magnet to the analyte solution, thereby improving overall colorimetric LFIA sensitivity. This effect has been explored within core-shell and satellite magnetic-plasmonic nanoparticle systems. For example, Yang et al. utilized gold nanoparticle-decorated Fe_3O_4 nanospheres, reporting enhanced colorimetric detection[44]. Additionally, Li et al. developed Fe_3O_4 nanoclusters, conjugated with gold nanoshells, observing improved visual readout[45]. Fe_3O_4-gold hetero-aggregates were also investigated by Razo et al. for colorimetric LFIA optimization[46]. Although hybrid Fe_3O_4-based gold nanoparticle systems improve LFIA sensitivity, their LSPR activity remains suboptimal due to the limitations of isotropic spherical gold nanoparticle design. We believe that incorporating an anisotropic nanoparticle system, such as a nanostar shell on the Fe_3O_4 core, leveraging the high optical brightness of anisotropic gold nanostars, can significantly enhance the sensitivity of colorimetric LFIA.

In this study, we developed a magneto-plasmonic enhanced mpLFIA assay by designing a novel nanoparticle system, mpGNS, which significantly improves colorimetric brightness and enhances LFIA performance through the synergistic effects of magnetic concentration and plasmonic enhancement provided by the gold nanostar shell surrounding the magnetic core. RVFV nucleoprotein was selected as a model analyte to evaluate the performance of the mpLFIA platform. Analysis of the colorimetric signal intensity at the test line revealed that mpGNS-3, characterized by its longest spikes and highest branch density, exhibited the highest analytical sensitivity. The limit of detection (LOD) for the RVFV nucleoprotein using mpGNS-3 was as low as 2.24 pg/mL, demonstrating a 1000-fold improvement in sensitivity compared to assays utilizing

conventional GNP. Moreover, our mpLFIA method was successfully applied to spiked blood serum samples, demonstrating significant potential for practical applications. We envision that this mpLFIA could serve not only for RVFV nucleoprotein detection but also as a versatile platform for detecting other infectious diseases in clinical samples.

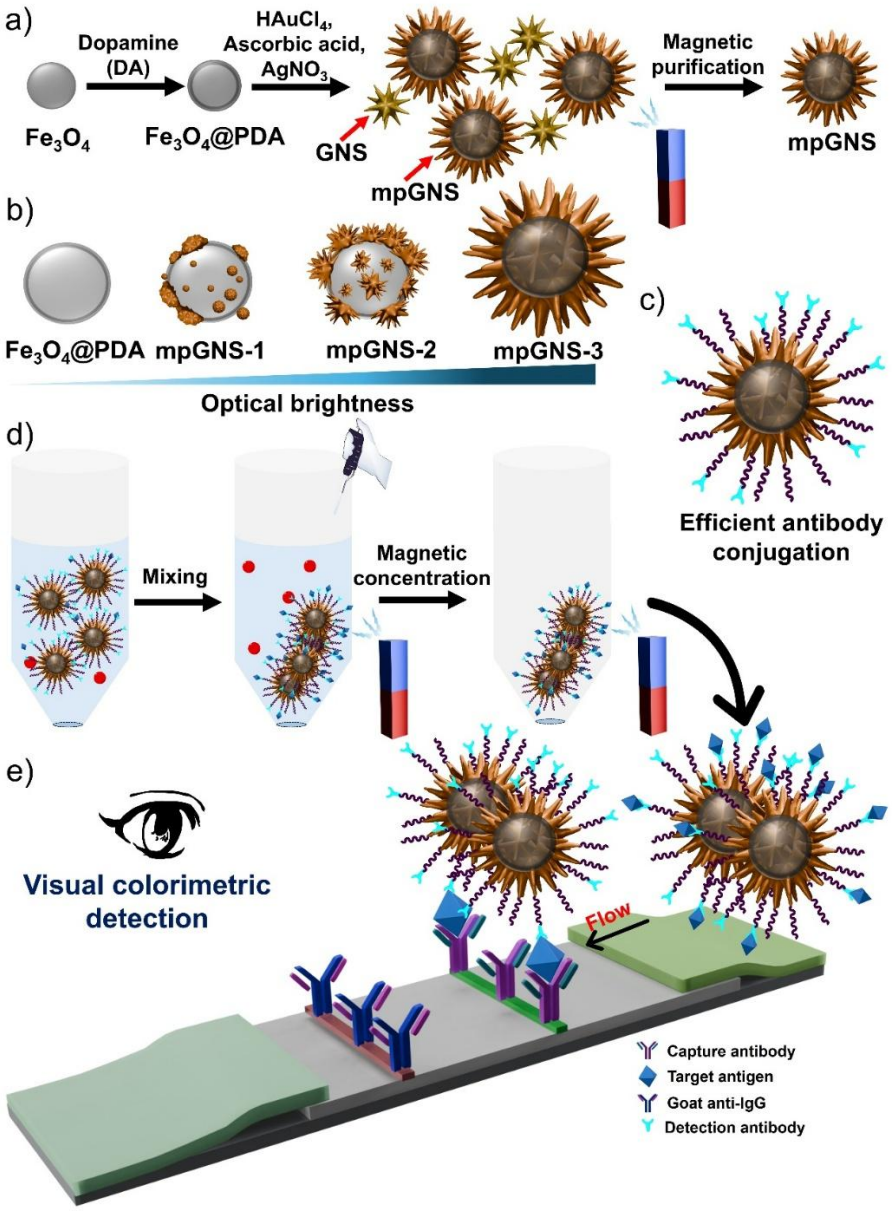

Figure 1. Schematic for the synthesis and purification of mpGNS (a). Optical brightness of the nanoparticle systems including Fe_3O_4@PDA, mpGNS-1, mpGNS-2, and mpGNS-3 (b). Efficient

antibody conjugation efficiency of the mpGNS-3 (c). Magnetic concentration of the mpGNS-3@ab with the RVFV nucleoprotein (d). Magneto-plasmonics enhanced visual colorimetric LFIA performance with mpGNS-3 (e).

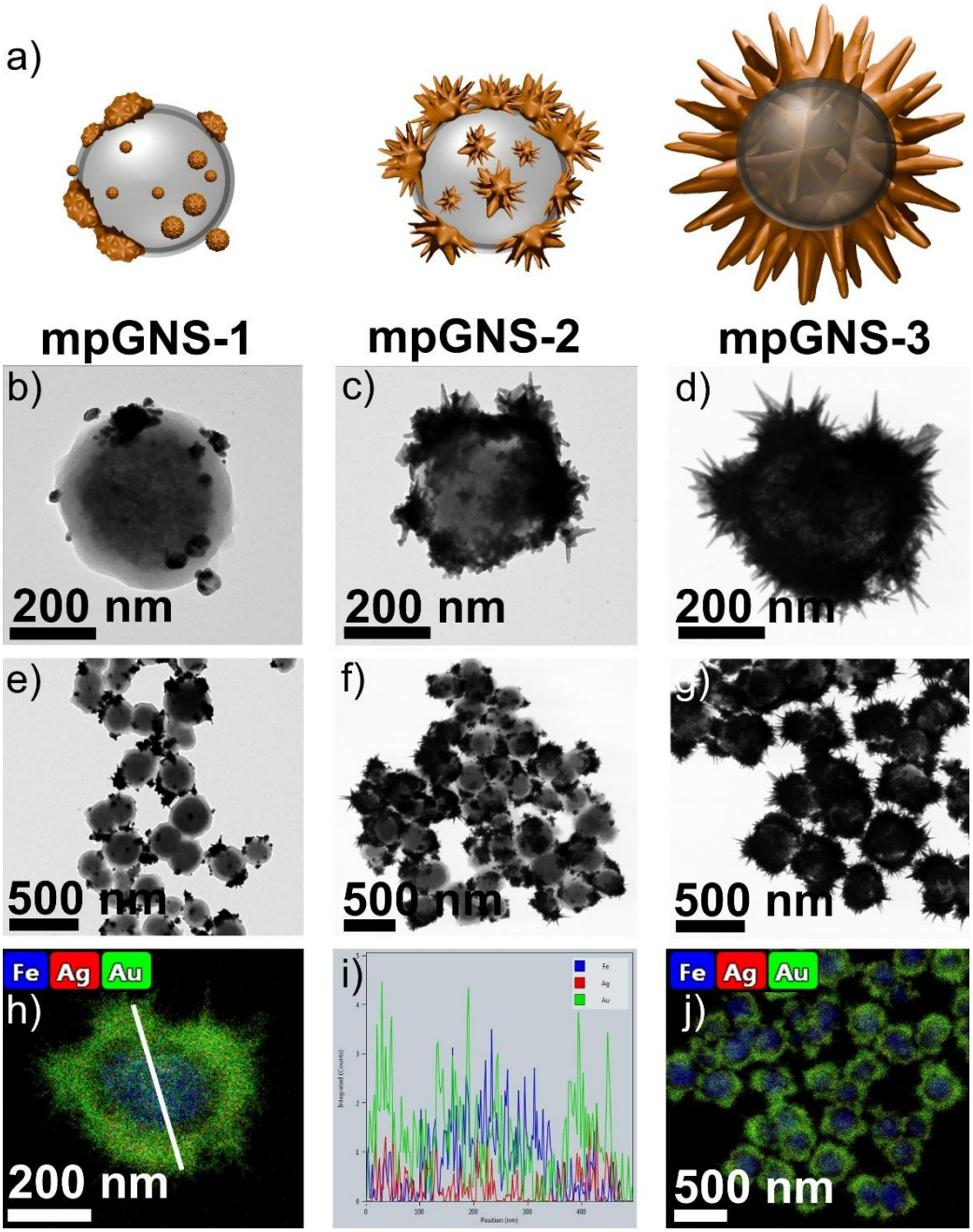

Figure 2. 3D model of the mpGNS (a). TEM images of the mpGNS-1, mpGNS-2, and mpGNS-3 (b-d). TEM images of the mpGNS-1, mpGNS-2, and mpGNS-3 with multiple number of

nanoparticles showing monodispersity of the nanoparticles (e-g). STEM-EDS image of the mpGNS-3 (h). STEM-EDS line profile showing Fe concentrated at the nanoparticle core, with Au and Ag distributed on the surface (i). STEM-EDS image of mpGNS-3 displaying multiple nanoparticles, highlighting their monodispersity (j).

Results and discussions

Working principle of the magneto-plasmonics enhanced LFIA platform using mpGNS

In this study, we integrated two amplification mechanisms to enhance colorimetric LFIA: (1) analyte concentration within the sample, driven by the iron oxide core, and (2) enhanced optical brightness, achieved through the sharp spiked morphology of the outer shell of the nanoparticle system. To achieve the Fe_3O_4 core with a sharp-spiked shell morphology, we developed a simple and straightforward surfactant-free synthesis strategy to fabricate iron core-gold nanostar (mpGNS) structures with numerous sharp branches. Establishing a surfactant-free synthesis method is essential for maximizing spike formation and enhancing colorimetric LFIA performance. In contrast, surfactant-based methods can obstruct nucleation centers, inhibiting spike development[47]. While previous studies have explored magnetic core-shell gold nanostars, many have relied on complex synthesis procedures involving surfactants[48, 49]. In this study, we present a surfactant-free approach specifically designed to optimize spike formation, achieving the highest possible number of sharp branches.

Figure 1a presents a schematic representation of the two-step synthesis and purification process of mpGNS. In the first step, Fe_3O_4 seeds were coated with polydopamine (PDA), which enhances gold deposition and formation of spikes. In the second step, mpGNS was synthesized and purified by adding $HAuCl_4$, $AgNO_3$, and ascorbic acid in a 2:2:1 ratio. To obtain different mpGNS

morphologies (mpGNS-1, mpGNS-2, and mpGNS-3), three distinct concentrations of these reagents were used while maintaining the fixed ratio. Notably, this surfactant-free synthesis method results in gold nanostar impurities, which can be effectively removed via magnetic purification. **Figure 1b** displays 3D models of the mpGNS structure and its various morphologies. The mpGNS were functionalized with the detection antibody for the RVFV protein using a classical NHS-coupling procedure. Among the three morphologies, mpGNS-3, which possesses a higher number of branches, exhibited enhanced antibody conjugation efficiency (**Figure 1c**). **Figure 1d** illustrates the schematic representation of the mpLFIA platform based on mpGNS for RVFV protein detection. This platform operates through a two-step process (**Figure 1e**). In the first step, mpGNS-3@dAb was mixed with RVFV-containing blood serum, and the nanoparticles were concentrated magnetically. In the second step, LFIA was performed by placing the mpGNS-3@dAb with bound RVFV nucleoprotein onto the conjugate pad of an LFIA strip. Upon encountering the target RVFV protein, the mpGNS-3@dAb complexes were captured by immobilized RVFV-specific capture antibodies on the test line, generating an intense dark bluish-green signal.

Characterization of mpGNS

Figure S1 presents the TEM image of Fe_3O_4@PDA, revealing an average seed size of 300 ± 60 nm. **Figure S2** displays the TEM image of the mpGNS-3 system synthesized at a 2:2:1 chemical ratio, showing the formation of two distinct types of nanostars-small and large. Given that the core of mpGNS reached approximately 202 nm, we inferred that the smaller nanostars were gold nanostars, likely impurities. To eliminate these impurities, we conducted magnetic separation, which successfully removed the small gold nanostars, as confirmed by the absence of small nanostars in the purified sample. **Figure 2a** presents 3D models of the mpGNS nanoparticles, while

Figure 2b-d display STEM images of mpGNS-1, mpGNS-2, and mpGNS-3 after purification. The STEM images of mpGNS further confirm structural homogeneity having large core size and gold shell (**Figure 2e-g**). To investigate the elemental distribution of the mpGNS-3 nanoparticles, we performed energy-dispersive X-ray (EDX) spectroscopy (**Figure 2h**), confirming that Fe is localized at the core, while Au and Ag are distributed on the surface. The elemental line profile of mpGNS-3 further supports this distribution, validating the successful formation of the magnetic-plasmonic nanostructure. Additionally, the STEM-EDX image of multiple mpGNS-3 nanoparticles demonstrates a highly monodisperse morphology, with Fe confined to the core and Au and Ag coating the surface (**Figure 2i**). The absorbance spectra of the nanoparticles reveal that the plasmon peak of mpGNS is red shifted from 544 nm to the 1054 nm range (**Figure 3a**). As expected, the formation of sharp branches on the mpGNS increases progressively from mpGNS-1 to mpGNS-3, resulting in stronger LSPR effects. Consequently, the absorbance peak undergoes a red shift, and the peak intensity significantly increases compared to that of the iron oxide nanoparticles.

LFIA performance of mpGNS

Figure 3b (top) presents a photograph of mpGNS and Fe_3O_4@PDA nanoparticles at an Fe concentration of 30 µg/mL, as determined by ICP-MS analysis. The image indicates that mpGNS-3 exhibits a darker color, signifying higher optical brightness compared to the other nanoparticles. As previously discussed, the anisotropic sharp-spiked morphology enhances the optical brightness of the nanoparticle system, with mpGNS-3 displaying the highest color intensity. We further evaluated the LFIA performance of the nanoparticle systems at the same concentration and conducted the LFIA assay at an RVFV nucleoprotein concentration of 2.5 ng/mL. **Figure 3b** (bottom) presents photographs of LFIA strips with different nanoparticle systems. **Figure 3c**

displays the gray value profile of the nanoparticle systems, while **Figure 3d** illustrates the gray value intensity of the test lines. The results show that the gray value intensity of mpGNS-3 was nearly twice as high as that of Fe_3O_4@PDA nanoparticles. This finding confirms that mpGNS-3, being a plasmonic-rich nanoparticle system, enhances optical brightness and significantly increases LFIA intensity.

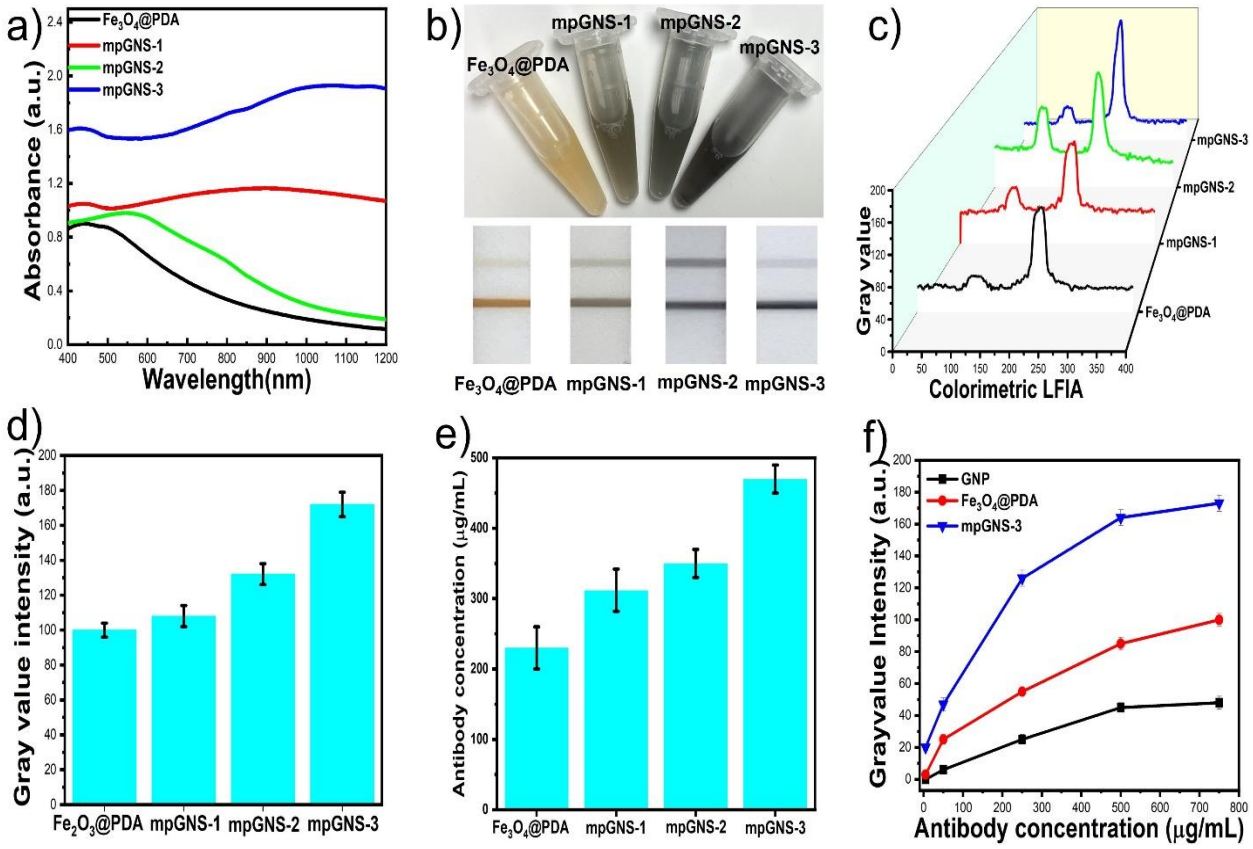

Figure 3. Absorbance spectra of the nanoparticles at the same concentration (a). Photograph of nanoparticle solutions at the same concentration and LFIA performance at 2.5 ng/mL RVFV nucleoprotein concentration (b). Gray value profile of LFIA strips with different nanoparticle systems (c). Gray value intensity of the test line for different nanoparticle systems (d). Antibody concentration across different nanoparticle systems (e). Gray value intensity profile at varying antibody concentrations for GNP, Fe_3O_4@PDA, and mpGNS-3 (f).

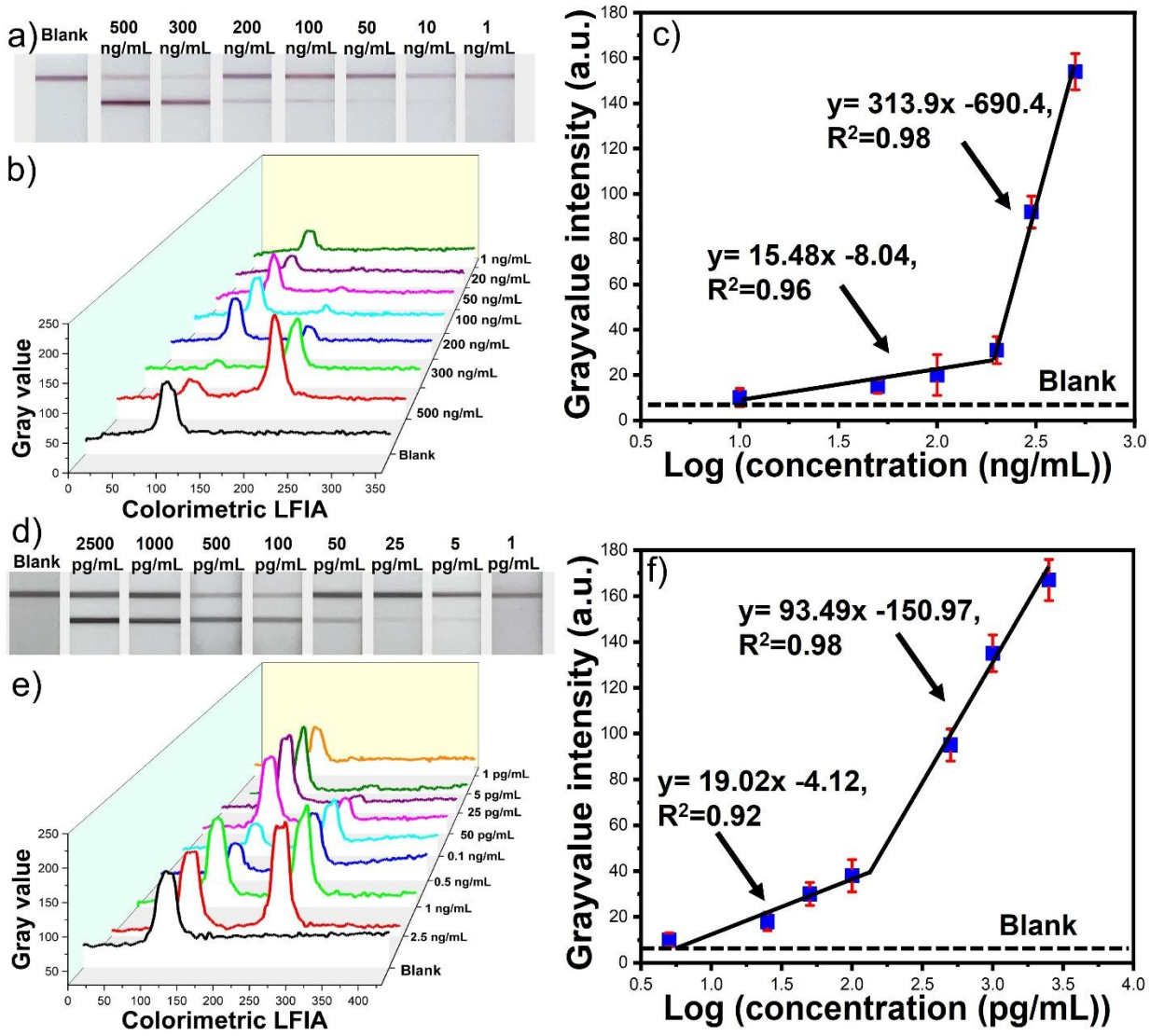

Figure 4. Photographs of the LFIA strips having GNP@ab with different concentration of RVFV nucleoprotein ranging from 500 ng/mL to 1 ng/mL (a). Gray value profile of the LFIA strips at different concentrations of RVFV nucleoprotein concentrations, ranging from 500 ng/mL to 1 ng/mL (b). Calibration curve of GNP showing two distinct linear correlations between gray value intensities and the logarithm of RVFV nucleoprotein concentrations (c). Photographs of the LFIA strips having mpGNS-3@ab with different concentration of RVFV nucleoprotein ranging from 2.5 ng/mL to 1 pg/mL (d). Gray value profile of LFIA strips at varying RVFV nucleoprotein concentrations, ranging from 2.5 ng/mL to 1 pg/mL (e). Calibration curve of mpGNS-3 showing

two distinct linear correlations between gray value intensities and the logarithm of RVFV nucleoprotein concentrations (f).

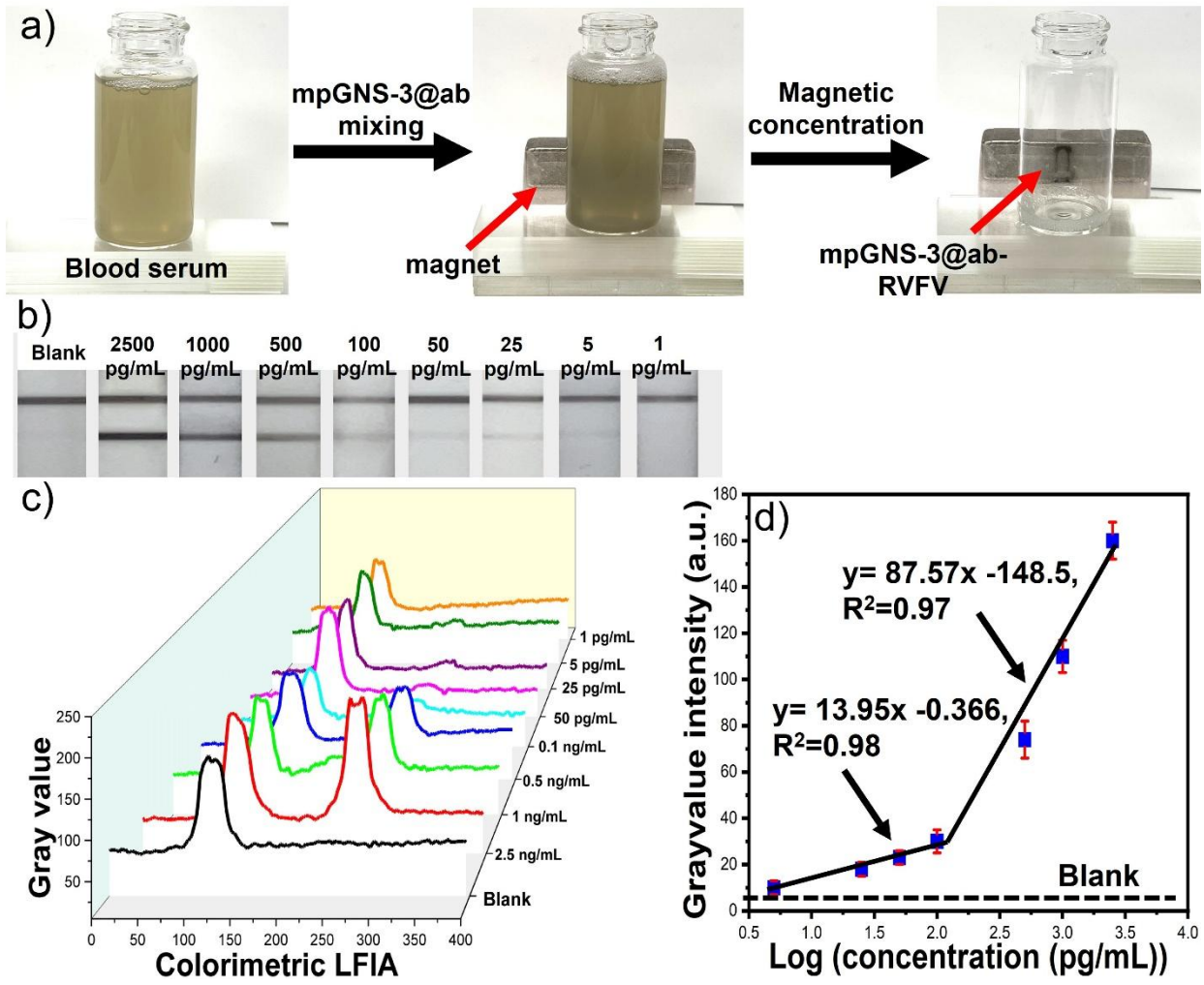

Figure 5. Magnetic concentration process for blood serum spiked samples with mpGNS-3@ab (a). Photographs of LFIA strips containing mpGNS-3@ab at varying concentrations of blood serum-spiked RVFV nucleoprotein, ranging from 2.5 ng/mL to 1 pg/mL (b). Gray value profile of the LFIA strips at different concentrations of RVFV nucleoprotein concentrations, ranging 2.5 ng/mL to 1 pg/mL (c). Calibration curve of mpGNS-3 showing two distinct linear correlations between gray value intensities and the logarithm of RVFV nucleoprotein concentrations (d).

We evaluated the antibody coupling efficiency of the nanoparticles by measuring the antibody concentration using absorbance analysis of the detection antibodies bound to mpGNS. As shown in **Figure 3e**, mpGNS-3 exhibited a higher coupling efficiency (70 %) compared to Fe_3O_4@PDA (35 %), demonstrating its effectiveness as a target antibody-labeling LFIA platform. As expected, the multiple sharp branches of mpGNS-3 increase the surface area of the nanoparticle system, thereby enhancing antibody conjugation efficiency relative to other mpGNS variants and Fe_3O_4@PDA. We compared the gray value intensity of mpGNS-3 with traditional GNP and Fe_3O_4@PDA at an RVFV nucleoprotein concentration of 200 ng/mL across different detection antibody concentrations ranging from 5 µg/mL to 750 µg/mL (**Figure 3f**). The LFIA assay was performed with magnetic concentration for mpGNS-3 and Fe_3O_4@PDA, while GNP underwent a traditional colorimetric LFIA assay without magnetic concentration, as it lacks magnetic properties. The results indicate that gray value intensity increased with higher detection antibody concentrations, reaching a maximum at approximately 750 µg/mL. Notably, mpGNS-3 exhibited the highest gray value intensity compared to GNP and Fe_3O_4@PDA. As expected, mpGNS-3 leverages both strong plasmonic effects, which enhance the color intensity of the LFIA test line, and magnetic concentration, which increases analyte accumulation, thereby achieving greater LFIA sensitivity than Fe_3O_4@PDA and traditional GNP.

mpLFIA Performance with mpGNS-3

Given that mpGNS-3 exhibits optimal morphology for maximum color brightness, we next evaluated its colorimetric detection sensitivity across RVFV nucleoprotein concentrations and compared its performance with that of traditional GNP-based LFIA. To quantify the detection performance, the calibration curve was constructed by plotting the average grayscale values of the test line against the RVFV concentrations. **Figure 4a** presents the colorimetric visualization of

LFIA strips for GNP at RVFV nucleoprotein concentrations ranging from 500 ng/mL to 1 ng/mL. The corresponding gray value intensity profiles are shown in **Figure 4b**. **Figure 4c** presents the calibration curve, which correlates the gray value intensity of the test lines with the logarithm of RVFV protein concentration. Two distinct linear regions were identified: one ranging from 500 ng/mL to 200 ng/mL and the other from 200 ng/mL to 10 ng/mL. The limit of detection (LOD) was determined using the International Union of Pure and Applied Chemistry (IUPAC) definition: $LOD = 3\sigma/S$, where σ is the standard deviation of blank measurements and S is the slope of the linear equation in the low concentration range (200 ng/mL to 10 ng/mL). The calculated LOD for GNP was as low as 2 ng/mL. For mpGNS-3, the LFIA strip images exhibit clear visual detection at nanogram-level RVFV concentrations, with the test line remaining visible even at a concentration of 5 pg/mL. This result highlights its superior colorimetric detection capability compared to GNP. **Figure 4d** displays the colorimetric visualization of LFIA strips for mpGNS-3 at RVFV nucleoprotein concentrations ranging from 2.5 ng/mL to 1 pg/mL, with the corresponding gray value intensity profiles shown in **Figure 4e**. The analytical calibration curve for mpGNS-3, illustrated in **Figure 4f**, was generated by plotting the averaged grayscale values of the test line against the logarithm of RVFV nucleoprotein concentrations. Two distinct linear regions were identified: one spanning 2.5 ng/mL to 100 pg/mL and another covering 100 pg/mL to 5 pg/mL. The calculated LOD for mpGNS-3 reached an impressive 2.24 pg/mL. These findings demonstrate that the mpLFIA platform achieves nearly a 1000-fold increase in sensitivity compared to traditional colorimetric detection with GNP, underscoring the superior performance of mpLFIA with mpGNS-3. As expected, mpGNS-3 exhibited greater temperature changes, attributed to its enhanced LSPR effect, which significantly improves its optical properties and detection efficiency.

Table 1. Literature review of magneto-plasmonics nanoparticle systems for colorimetric LFIA.

Nanoparticle System	LOD	Reference
Fe_3O_4@Au NPs	10 ng mL^{-1}	[44]
Fe_3O_4-AgMBA@Au nanoparticles	0.1 ng mL^{-1}	[50]
Gold NP-conjugated magnetic bead (GMB)	0.1 ng mL^{-1}	[51]
Magnetic and Gold NP Heteroaggregates	0.25 ng mL^{-1}	[46]
Au Nanoshell-Loaded Fe_3O_4 Nanoclusters	1 ng mL^{-1}	[45]
mpGNS-3	**1.7 pg mL^{-1}**	**This work**

mpLFIA performance with RVFV nucleoprotein spiked blood serum and stability of the mpGNS-3 probe

We further assessed the real-world applicability of the proposed mpLFIA by performing the LFIA assay with RVFV spiked into a blood serum sample, without any purification or dilution. **Figure 5a** illustrates the magnetic concentration process using blood serum samples spiked with RVFV nucleoprotein. **Figure 5b** presents photographs of the LFIA strips at various RVFV nucleoprotein concentrations in blood serum, ranging from 2.5 ng/mL to 1 pg/mL, while **Figure 5c** displays the corresponding gray value intensity profiles. Consistent with previous measurements, a linear correlation was observed within the logarithmic concentration range of 500 ng/mL to 5 pg/mL **(Figure 5c)**. The LOD for the spiked in blood serum samples was determined to be as low as 1.17 pg/mL, demonstrating that the proposed mpLFIA enables highly sensitive and quantitative detection of infectious diseases in real-world applications without requiring any sample preparation.

We evaluated the stability of the mpGNS-3@ab probe by examining its morphology after six months of storage in a standard refrigerator at 2-8 ºC. **Figure 6a** displays LFIA strip images taken at two-week intervals over six months using the mpGNS-3 probe with a 500 ng/mL concentration

of the RVFV nucleoprotein. **Figure 6b** illustrates the gray value intensities at the test line, which shows a relative standard deviation (RSD) of 6.5 %, confirming the high stability and long-term usability of the photothermal LFIA probe. **Figure 6c** presents the absorbance spectra of mpGNS immediately after synthesis and after six months of storage, demonstrating the LSPR stability of the nanoparticles. Additionally, **Figure 6d-g** shows the STEM-EDS image of the mpGNS-3 probe after the storage period, confirming that its sharp spike morphology and Fe core remained well-preserved.

Furthermore, we compared the performance of our mpLFIA with previously reported colorimetric sensing approaches that utilize magneto-plasmonics nanoparticle systems (**Table 1**). The results demonstrate that mpGNS-3 achieves the highest colorimetric efficiency and significantly improved LFIA sensitivity compared to existing colorimetric LFIA probes. By integrating magnetic concentration of larger sample volumes with plasmonic enhancement-enabled by the gold nanostar shell coating, the magnetic core-mpGNS-3 surpasses traditional LFIA approaches based on gold nanospheres and other nanoparticle systems. Ultimately, these findings confirm that the mpGNS-3 probe offers superior colorimetric enhancement, excellent antibody conjugation efficiency, and long-term stability, making it a highly effective tool for sensitive LFIA detection.

Overall, we demonstrate that the mpLFIA platform provides a highly sensitive and quantitative approach for infectious disease detection, offering a cost-effective solution for large-scale screening. Notably, it requires only a magnet to concentrate the nanoparticle system and a visual colorimetric probe: mpGNS-3, making it a practical and accessible tool for point-of-care diagnostics in low-resource settings. Its simplicity and efficiency make it particularly suited for early disease detection before hospital admission, helping to curb the spread of infections in densely populated areas.

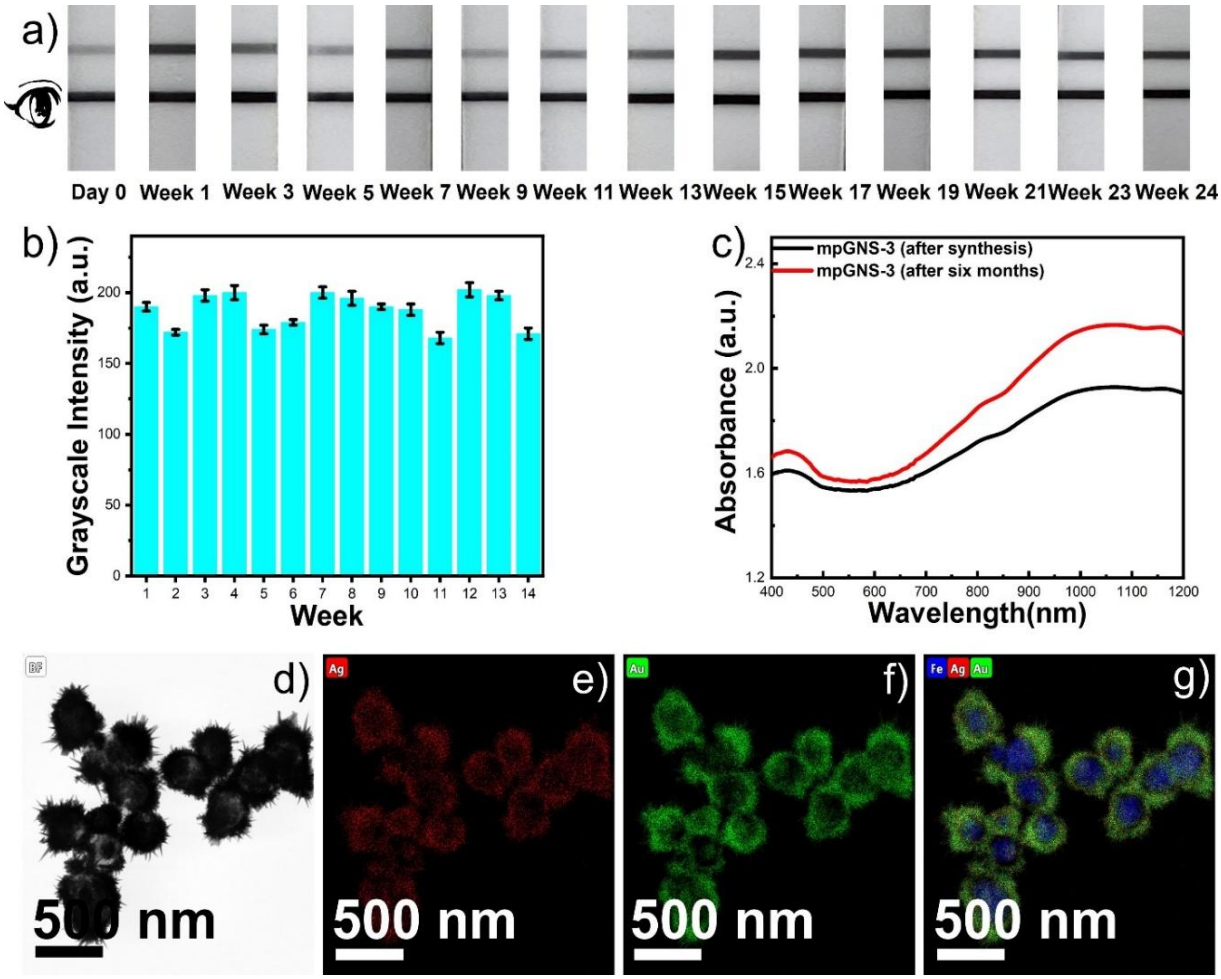

Figure 6. 3D model of the mpGNS (a). TEM images of the mpGNS-1, mpGNS-2, and mpGNS-3 (b-d). TEM images of the mpGNS-1, mpGNS-2, and mpGNS-3 with multiple number of nanoparticles showing monodispersity of the nanoparticles (e-g). STEM-EDS image of the mpGNS-3 (h). STEM-EDS line profile showing Fe concentrated at the nanoparticle core, with Au and Ag distributed on the surface (i). STEM-EDS image of mpGNS-3 displaying multiple nanoparticles, highlighting their monodispersity (j).

Conclusion

In this work, we introduce a breakthrough strategy for synthesizing magneto-plasmonic gold nanostars (mpGNS) as a next-generation colorimetric signal tag, revolutionizing LFIA technology.

Our approach enables highly efficient antibody conjugation while dramatically improving upon performance of colorimetric LFIA, by harnessing the synergistic effects of magnetic enrichment and plasmonic signal amplification. Our mpGNS-3-based LFIA system achieves an unprecedented detection limit of 2.24 pg/mL for RVFV nucleoprotein, demonstrating exceptional analytical sensitivity. Moreover, it maintains superior performance in complex biological matrices, successfully detecting RVFV nucleoprotein in blood serum without any pretreatment. This work not only provides a powerful blueprint for designing high-performance POCT diagnostics but also establishes an advanced nanoplatform for ultra-sensitive infectious disease detection. Beyond its immediate applications, our strategy lays the foundation for low-cost, scalable hybrid nanoparticle synthesis, opening new avenues for next-generation colorimetric LFIA platforms with transformative impact in global healthcare and epidemic preparedness.

By integrating cutting-edge nanomaterials with a user-friendly LFIA format, our mpLFIA technology represents a transformative advancement in POCT diagnostics. With its unparalleled sensitivity, portability, and adaptability to diverse biomarkers, this platform holds immense potential for early infectious disease detection, outbreak surveillance, and resource-limited settings where rapid, ultra-sensitive diagnostics are critical.

Experimental section

Materials and instruments

200 nm carboxylated iron (III) oxide (Fe_3O_4) nanoparticles (10mg/mL) were purchased from BOC Sciences. Dopamine hydrochloride, tris(hydroxymethyl)aminomethane (Tris buffer) solution, chloroauric acid ($HAuCl_4$), ascorbic acid, 1 mM hydrochloric acid (HCl) solution, trisodium citrate, hexadecyltrimethylammonium chloride (CTAC) solution 25% (w/v) in water, 10x

phosphate buffer solution (PBS), TWEEN-20, and bovine serum albumin (BSA) were purchased from Sigma-Aldrich. Milli-Q deionized (DI) water was used throughout the experiment. SH-PEG-NHS (Mw 5k) (mPEG) was purchased from NANOCS. N52 Neodymium block magnets were purchased from K&J Magnets Inc. The morphology of mpGNS was characterized using the Aberration Corrected STEM-Thermo Fisher Titan 80-300 Microscope. UV-vis spectra were recorded using a Shimadzu UV-3600i spectrometer with cuvettes of 1-cm path length at room temperature. A smartphone was used to capture images of LFIA strips.

Ethics Statement

All procedures involving animals were reviewed and approved by the Institutional Animal Care and Use Committee at the University of Nevada, Reno (Protocol #20-06-1026). Oversight of laboratory animal work was provided by the Office of Laboratory Animal Medicine, ensuring compliance with policies set forth by the National Institutes of Health Office of Laboratory Animal Welfare (Assurance # A3500-01).

Synthesis of Fe_3O_4@PDA seeds

250 µL of carboxylated Fe_3O_4 nanoparticles were diluted in 1.75 mL of Milli-Q water. The solution was centrifuged at 6,000 g for 10 minutes. After the supernatant was removed, the pellet was redispersed in 2 mL of Milli-Q water. 100 µL of CTAC was added to the sample, and the mixture was left to spin for 30 minutes. The nanoparticle solution was then centrifuged at 8,000 g for 5 minutes. After the removal of the supernatant, the pellet was redispersed in 1.5 mL DI water. 10 mg of dopamine hydrochloride was dissolved in 1 mL of Tris buffer to initiate polymerization. 500 µL of polydopamine (PDA) solution was added to the particles, and the mixture was left to spin overnight. After spinning, the particles were centrifuged three times at 6,000 g for 5 minutes. After

the first two washes, the supernatant was removed, and the pellet was redispersed in 1.5 mL of DI water and 50 µL of CTAC. After the third wash, the supernatant was removed, and the pellet was redispersed in 2 mL of DI water.

Synthesis of mpGNS

mpGNS was synthesized in 250-mL Erlenmeyer flasks and washed thoroughly with aqua regia. Within a flask containing Milli-Q water, with the approximate volume added to result in 50 mL, 200 µL of 1 M HCl was added. Subsequently, 125 µL of seeds were added, followed by the addition of $HAuCl_4$, $AgNO_3$, and ascorbic acid. $HAuCl_4$, $AgNO_3$, and ascorbic acid were added in a 2:2:1 ratio. The volumes of $HAuCl_4$ used in this experiment include 250 µL, 500 µL, and 2 mL. After a visual color change occurred from pale brown to dark bluish green color, 1 mL of CTAC solution was added to stabilize the particles. The solutions were transferred into 50 mL centrifuge tubes and left to spin for 30 minutes. After spinning, the nanoparticles were centrifuged at 4,000 g for 10 minutes. The supernatant was removed, and the pellet was redispersed in a mixture of 9 mL of Milli-Q water and 1 mL CTAC. After that, the mpGNS was magnetically purified to separate from gold nanostars impurity. After five minutes, the supernatant was removed, and the concentrated particles were combined into 1 mL of solution with Milli-Q water and mixed with mPEG-NHS-SH for further antibody functionalization.

Monoclonal antibody production

Female 8 week-old BALB/c and CD-1 mice (Charles River Laboratories Inc., Frederick, MA) were administered intraperitoneal immunizations with recombinant RVFV nucleoprotein (rNP) (BEI Resources, Manassas, VA) was emulsified in Freund's complete adjuvant (Millipore Sigma, Billerica, MA). Subsequent booster immunizations were delivered via intraperitoneal injections

using RVFV rNP (BEI Resources) emulsified with Freund's incomplete adjuvant (Millipore Sigma). Blood samples were collected through retro-orbital bleeds, and serum was separated using Microtainer serum separator tubes (Becton, Dickinson and Copmany, Franklin Lakes, NJ). Antibody titers were determined using indirect ELISAs, where RVFV rNP (The Native Antigen Company, Kidlington, United Kingdom) was immobilized onto assay plates. Splenocytes were harvested from immunized mice, and hybridoma fusion was carried out following a standard protocol. Monoclonal antibodies were subsequently purified from hybridoma cell culture supernatants via protein A affinity chromatography.

Recombinant RVFV NP Expression and Purification

Additional recombinant antigen for assay development and validation was produced in-house by the AuCoin laboratory. The RVFV MP12 strain NP sequence was retrieved from GenBank (accession number AF134530.1). This sequence, including an N-terminal GS linker and poly-histidine tag, was cloned into the pcDNA3.4 vector by GenScript Biotech. The resulting plasmid was transformed into *Escherichia coli* (*E. coli*) strain NEB 5α (New England Biolabs, Ipswich, MA). Plasmid DNA was extracted using the ZymoPURE II plasmid maxiprep kit (Zymo Research, Irvine, CA). Prior to transfection into mammalian cells, plasmid integrity was confirmed via sequencing. Purified DNA was then used to transfect Expi293 cells (Thermo Fisher Scientific, Waltham, MA) employing the ExpiFectamine 293 transfection kit (Thermo Fisher Scientific). Seven days after transfection, rNP was isolated via His-Pur Cobalt Resin (Thermo Fisher Scientific). The purified RVFV rNP was characterized through Coomassie staining and Western blot analysis. Additionally, quantification of AuCoin lab-produced RVFV rNP was achieved using antigen-capture ELISA, with a standard curve generated from commercially available RVFV NP (The Native Antigen Conpany). Protein stocks were stored at -80 °C until required.

Synthesis of mpGNS and GNP-probe

The synthesis of antibody-conjugated GNP and mpGNS was performed as follows: briefly, a 1-mL solution of mpGNS was centrifuged at 5000 g for 10 minutes and resuspended in 1 mL 1 mM of SH-PEG-NHS (Mw-5k). The solution was mixed for one hour at room temperature, then centrifuged at 4000g for 5 minutes. The resulting pellet was re-suspended in 1 mL of PBS with 0.01 % Tween-20 buffer and incubated with the detection antibody RVFV at a concentration of 500 µg/mL at 4°C for 24 hours. Then, the solution was centrifuged again at 4000g for 5 minutes and re-suspended in a mixture of 200 µL of 10% Tween-20 and 800 µL of 3% (w/v) BSA. The solution was then stored at 4°C for subsequent assay analysis. The final concentrations of mpGNS and Fe_3O_4@PDA nanoparticles were adjusted so that the Fe concentration in the nanoparticle solution was 100 µg/mL, as determined by ICP-MS analysis.

To conjugate traditional GNP with the detection antibody, we first synthesized the GNP using a previously reported method[16]. Subsequently, 10 mL of the synthesized GNP solution was functionalized by adding 5 µL of a 100 mM CTAC solution. The mixture was incubated for one hour and subsequently centrifuged at 8000g for 15 minutes. The resulting pellet was resuspended in water and further functionalized with 1 mL of 1 mM SH-PEG-NHS (Mw 5k). After a one-hour incubation at room temperature, the solution was centrifuged at 5000g for 12 minutes. The pellet was then resuspended in 1 mL of PBS (10x, pH 7.4) buffer and incubated with the RVFV detection antibody at a concentration of 500 µg/mL at 4°C for 24 hours. Following incubation, the solution was centrifuged again at 5000g for 12 minutes and resuspended in a stabilizing mixture containing 500 µL of 10% Tween-20 and 500 µL of 3% (w/v) BSA. The final conjugate solution was stored at 4°C for subsequent assay analysis.

Preparation of LFIA strips

The LFIA strips were assembled using a 8980 conjugate pad (Ahlstrom, Helsinki, Finland), a UniSart CN95 nitrocellulose membrane (Sartorius, Germany), and a CFSP203000 absorbent wicking pad (EMD Millipore, Billerica,MA), all mounted onto an adhesive backing card (DCN Dx, Carlsbad, CA). The conjugate pad was pre-treated with a blocking buffer consisting of 10 mM borate buffer and 0.25% Triton X-100 (Sigma Aldrich, St. Louis, MS). The nitrocellulose membrane was pre-treated with a blocking buffer containing 10 mM sodium phosphate, 0.1% bovine serum albumin (BSA) (Sigma Aldrich), 0.2% PVP-40 (Sigma Aldrich), and 0.1% sucrose (Sigma Aldrich). The BioDotXYZ3060 was implemented in the striping of nitrocellulose membranes. The capture antibody of the RVFV LFIA was dispensed on the test line at a concentration of 1.0 mg/mL, while goat anti-mouse IgG polyclonal antibodies (Southern Biotech, USA) were applied to the control line at 1 mg/mL. Finally, the strips were cut to a width of 4 mm.

mpLFIA prototype for RVFV nucleoprotein detection

To evaluate the effectiveness of mpLFIA using mpGNSs, the assay was first evaluated with varying concentrations of RVFV nucleoprotein spiked into buffer (1X PBS). For each assay, 20 mL of the RVFV nucleoprotein in buffer was mixed with 100 µL of mpGNS@ab probes, followed by a 5-minute incubation and magnetic concentration of the nanoparticles for an additional 5 minutes. Next, we combined 100 µL of 0.1% (1X PBS) containing 0.01% Tween-20 with the nanoparticles, applied the mixture to the sample pad of the LFIA strip, and allowed it to run for 10 minutes. Then, 200 µL of running buffer (0.01% Tween-20 in 0.1% 1 X PBS) was added to facilitate nanoparticle migration from the sample pad to the wicking pad over 10-15 minutes. For GNSP, we introduced 100 µL of the RVFV nucleoprotein solution onto the sample pad and conducted the assay. For blood serum samples, RVFV protein was spiked into 20 mL of blood serum. After magnetic concentration of the nanoparticles for 5 minutes, we mixed the nanoparticles with 100 µL of 0.1

% (1X PBS) containing 0.01% Tween-20 and applied onto the sample pad of the LFIA strip and run for 10 minutes. Then, 200 µL of running buffer (0.01% Tween-20 in 0.1% 1 X PBS) was added to facilitate nanoparticle migration from the sample pad to the wicking pad over 10-15 minutes. Subsequently, 200 µL of running buffer (0.01% Tween-20 in 0.1% 1X PBS) was added, allowing the nanoparticles to flow across the membrane for an additional 10-15 minutes, from the sample pad to the wicking pad. LFIA strips were imaged using a smartphone, and the grayscale intensity of the test line was digitized and analyzed using ImageJ.

Acknowledgments

This work was supported by the Chemical Biological Technologies Directorate contract [CONTRACT # MCDC-2019-693] from the Department of Defense Chemical and Biological Defense program through the Defense Threat Reduction Agency (DTRA), and the Bill and Melinda Gates Foundation (INV-040790).

Conflict of Interest

The authors declare no conflict of interest.

References

[1] Katarzyna M. Koczula, A. Gallotta, Lateral flow assays, Essays in Biochemistry 60(1) (2016) 111-120.
[2] N. Jiang, N.D. Tansukawat, L. Gonzalez-Macia, H.C. Ates, C. Dincer, F. Güder, S. Tasoglu, A.K. Yetisen, Low-Cost Optical Assays for Point-of-Care Diagnosis in Resource-Limited Settings, ACS Sensors 6(6) (2021) 2108-2124.
[3] W. Jung, J. Han, J.-W. Choi, C.H. Ahn, Point-of-care testing (POCT) diagnostic systems using microfluidic lab-on-a-chip technologies, Microelectronic Engineering 132 (2015) 46-57.
[4] P.B. Luppa, C. Müller, A. Schlichtiger, H. Schlebusch, Point-of-care testing (POCT): Current techniques and future perspectives, TrAC Trends in Analytical Chemistry 30(6) (2011) 887-898.
[5] C.M. Pandey, S. Augustine, S. Kumar, S. Kumar, S. Nara, S. Srivastava, B.D. Malhotra, Microfluidics Based Point-of-Care Diagnostics, Biotechnology Journal 13(1) (2018) 1700047.

[6] F. Di Nardo, M. Chiarello, S. Cavalera, C. Baggiani, L. Anfossi, Ten Years of Lateral Flow Immunoassay Technique Applications: Trends, Challenges and Future Perspectives, Sensors (Basel) 21(15) (2021).
[7] Y. Zhang, I.D. McKelvie, R.W. Cattrall, S.D. Kolev, Colorimetric detection based on localised surface plasmon resonance of gold nanoparticles: Merits, inherent shortcomings and future prospects, Talanta 152 (2016) 410-422.
[8] N.A. Byzova, A.V. Zherdev, B.N. Khlebtsov, A.M. Burov, N.G. Khlebtsov, B.B. Dzantiev, Advantages of Highly Spherical Gold Nanoparticles as Labels for Lateral Flow Immunoassay, Sensors 20(12) (2020) 3608.
[9] B.N. Khlebtsov, R.S. Tumskiy, A.M. Burov, T.E. Pylaev, N.G. Khlebtsov, Quantifying the Numbers of Gold Nanoparticles in the Test Zone of Lateral Flow Immunoassay Strips, ACS Applied Nano Materials 2(8) (2019) 5020-5028.
[10] F. Di Nardo, M. Chiarello, S. Cavalera, C. Baggiani, L. Anfossi, Ten Years of Lateral Flow Immunoassay Technique Applications: Trends, Challenges and Future Perspectives, Sensors 21(15) (2021) 5185.
[11] S. Zhang, Y. Moustafa, Q. Huo, Different Interaction Modes of Biomolecules with Citrate-Capped Gold Nanoparticles, ACS Applied Materials & Interfaces 6(23) (2014) 21184-21192.
[12] Y. Liu, L. Zhan, Z. Qin, J. Sackrison, J.C. Bischof, Ultrasensitive and Highly Specific Lateral Flow Assays for Point-of-Care Diagnosis, ACS Nano 15(3) (2021) 3593-3611.
[13] L. Zhan, S.-z. Guo, F. Song, Y. Gong, F. Xu, D.R. Boulware, M.C. McAlpine, W.C.W. Chan, J.C. Bischof, The Role of Nanoparticle Design in Determining Analytical Performance of Lateral Flow Immunoassays, Nano Letters 17(12) (2017) 7207-7212.
[14] J. Park, Lateral Flow Immunoassay Reader Technologies for Quantitative Point-of-Care Testing, Sensors 22(19) (2022) 7398.
[15] M. Supianto, H.J. Lee, Recent research trends in fluorescent reporters-based lateral flow immunoassay for protein biomarkers specific to acute myocardial infarction, Bulletin of the Korean Chemical Society 43(1) (2022) 4-10.
[16] S. Atta, Y. Zhao, S.V. Yampolsky, S. Sanchez, T. Vo-Dinh, Nanoengineered plasmonics-enhanced photothermal tags for sensitive detection of cardiac biomarker troponin I using lateral flow immunoassay, Chemical Engineering Journal 496 (2024) 153327.
[17] S. Atta, Y. Zhao, J.Q. Li, T. Vo-Dinh, Dual-Modal Colorimetric and Surface-Enhanced Raman Scattering (SERS)-Based Lateral Flow Immunoassay for Ultrasensitive Detection of SARS-CoV-2 Using a Plasmonic Gold Nanocrown, Analytical Chemistry 96(12) (2024) 4783-4790.
[18] M. Sánchez-Purrà, B. Roig-Solvas, C. Rodriguez-Quijada, B.M. Leonardo, K. Hamad-Schifferli, Reporter Selection for Nanotags in Multiplexed Surface Enhanced Raman Spectroscopy Assays, ACS Omega 3(9) (2018) 10733-10742.
[19] A.-C. Mirica, D. Stan, I.-C. Chelcea, C.M. Mihailescu, A. Ofiteru, L.-A. Bocancia-Mateescu, Latest Trends in Lateral Flow Immunoassay (LFIA) Detection Labels and Conjugation Process, Frontiers in Bioengineering and Biotechnology 10 (2022).
[20] F. Gao, Y. Wu, C. Gan, Y. Hou, D. Deng, X. Yi, Overview of the Design and Application of Photothermal Immunoassays, Sensors 24(19) (2024) 6458.
[21] S. Sloan-Dennison, E. O'Connor, J.W. Dear, D. Graham, K. Faulds, Towards quantitative point of care detection using SERS lateral flow immunoassays, Analytical and Bioanalytical Chemistry 414(16) (2022) 4541-4549.
[22] H. Tong, C. Cao, M. You, S. Han, Z. Liu, Y. Xiao, W. He, C. Liu, P. Peng, Z. Xue, Y. Gong, C. Yao, F. Xu, Artificial intelligence-assisted colorimetric lateral flow immunoassay for sensitive and quantitative detection of COVID-19 neutralizing antibody, Biosensors and Bioelectronics 213 (2022) 114449.

[23] C. Liu, Q. Jia, C. Yang, R. Qiao, L. Jing, L. Wang, C. Xu, M. Gao, Lateral Flow Immunochromatographic Assay for Sensitive Pesticide Detection by Using Fe3O4 Nanoparticle Aggregates as Color Reagents, Analytical Chemistry 83(17) (2011) 6778-6784.
[24] S. Bazsefidpar, A. Moyano, G. Gutiérrez, M. Matos, M.C. Blanco-López, Lipid–Polymer Hybrids Encapsulating Iron-Oxide Nanoparticles as a Label for Lateral Flow Immunoassays, Biosensors, 2021.
[25] L. Ge, D. Wang, F. Lian, J. Zhao, Y. Wang, Y. Zhao, L. Zhang, J. Wang, X. Song, J. Li, K. Xu, Lateral Flow Immunoassay for Visible Detection of Human Brucellosis Based on Blue Silica Nanoparticles, Frontiers in Veterinary Science 8 (2021).
[26] C.N. Loynachan, M.R. Thomas, E.R. Gray, D.A. Richards, J. Kim, B.S. Miller, J.C. Brookes, S. Agarwal, V. Chudasama, R.A. McKendry, M.M. Stevens, Platinum Nanocatalyst Amplification: Redefining the Gold Standard for Lateral Flow Immunoassays with Ultrabroad Dynamic Range, ACS Nano 12(1) (2018) 279-288.
[27] H.-K. Oh, K. Kim, J. Park, H. Im, S. Maher, M.-G. Kim, Plasmon color-preserved gold nanoparticle clusters for high sensitivity detection of SARS-CoV-2 based on lateral flow immunoassay, Biosensors and Bioelectronics 205 (2022) 114094.
[28] B. Gosselin, M. Retout, R. Dutour, L. Troian-Gautier, R. Bevernaegie, S. Herens, P. Lefèvre, O. Denis, G. Bruylants, I. Jabin, Ultrastable Silver Nanoparticles for Rapid Serology Detection of Anti-SARS-CoV-2 Immunoglobulins G, Analytical Chemistry 94(20) (2022) 7383-7390.
[29] M. Shin, W. Kim, K. Yoo, H.-S. Cho, S. Jang, H.-J. Bae, J. An, J.-c. Lee, H. Chang, D.-E. Kim, J. Kim, L.P. Lee, B.-H. Jun, Highly sensitive multiplexed colorimetric lateral flow immunoassay by plasmon-controlled metal–silica isoform nanocomposites: PINs, Nano Convergence 11(1) (2024) 42.
[30] T. Bai, L. Wang, M. Wang, Y. Zhu, W. Li, Z. Guo, Y. Zhang, Strategic synthesis of trimetallic Au@Ag–Pt nanorattles for ultrasensitive colorimetric detection in lateral flow immunoassay, Biosensors and Bioelectronics 208 (2022) 114218.
[31] Z. Zhang, H. Wang, Z. Chen, X. Wang, J. Choo, L. Chen, Plasmonic colorimetric sensors based on etching and growth of noble metal nanoparticles: Strategies and applications, Biosensors and Bioelectronics 114 (2018) 52-65.
[32] X. Huang, M.A. El-Sayed, Gold nanoparticles: Optical properties and implementations in cancer diagnosis and photothermal therapy, Journal of Advanced Research 1(1) (2010) 13-28.
[33] S.E. Skrabalak, J. Chen, Y. Sun, X. Lu, L. Au, C.M. Cobley, Y. Xia, Gold Nanocages: Synthesis, Properties, and Applications, Accounts of Chemical Research 41(12) (2008) 1587-1595.
[34] R.M.S.M. Baltar, S. Farooq, R.E. de Araujo, Selecting plasmonic nanoshells for colorimetric sensors, J. Opt. Soc. Am. B 40(4) (2023) C40-C47.
[35] N.M. Ngo, H.-V. Tran, T.R. Lee, Plasmonic Nanostars: Systematic Review of their Synthesis and Applications, ACS Applied Nano Materials 5(10) (2022) 14051-14091.
[36] H. de Puig, J.O. Tam, C.-W. Yen, L. Gehrke, K. Hamad-Schifferli, Extinction Coefficient of Gold Nanostars, The Journal of Physical Chemistry C 119(30) (2015) 17408-17415.
[37] F. Hao, C.L. Nehl, J.H. Hafner, P. Nordlander, Plasmon Resonances of a Gold Nanostar, Nano Letters 7(3) (2007) 729-732.
[38] T.V. Tsoulos, L. Han, J. Weir, H.L. Xin, L. Fabris, A closer look at the physical and optical properties of gold nanostars: an experimental and computational study, Nanoscale 9(11) (2017) 3766-3773.
[39] I.B. Becerril-Castro, I. Calderon, N. Pazos-Perez, L. Guerrini, F. Schulz, N. Feliu, I. Chakraborty, V. Giannini, W.J. Parak, R.A. Alvarez-Puebla, Gold Nanostars: Synthesis, Optical and SERS Analytical Properties, Analysis & Sensing 2(3) (2022) e202200005.
[40] S. Atta, A.J. Canning, R. Odion, H.-n. Wang, D. Hau, J.P. Devadhasan, A.J. Summers, M.A. Gates-Hollingsworth, K.J. Pflughoeft, J. Gu, D.C. Montgomery, D.P. AuCoin, F. Zenhausern, T. Vo-Dinh, Sharp

Branched Gold Nanostar-Based Lateral-Flow Immunoassay for Detection of Yersinia pestis, ACS Applied Nano Materials 6(5) (2023) 3884-3892.
[41] S. Atta, Y. Zhao, S. Sanchez, D. Seedial, J.P. Devadhasan, A.J. Summers, M.A. Gates-Hollingsworth, K.J. Pflughoeft, J. Gu, D.C. Montgomery, D.P. AuCoin, F. Zenhausern, T. Vo-Dinh, Plasmonic-Enhanced Colorimetric Lateral Flow Immunoassays Using Bimetallic Silver-Coated Gold Nanostars, ACS Applied Materials & Interfaces 16(40) (2024) 54907-54918.
[42] G. Armelles, A. Cebollada, A. García-Martín, M.U. González, Magnetoplasmonics: Combining Magnetic and Plasmonic Functionalities, Advanced Optical Materials 1(1) (2013) 10-35.
[43] G. Armelles, A. Cebollada, A. García-Martín, J.M. García-Martín, M.U. González, J.B. González-Díaz, E. Ferreiro-Vila, J.F. Torrado, Magnetoplasmonic nanostructures: systems supporting both plasmonic and magnetic properties, Journal of Optics A: Pure and Applied Optics 11(11) (2009) 114023.
[44] S. Yang, J. Du, M. Wei, Y. Huang, Y. Zhang, Y. Wang, J. Li, W. Wei, Y. Qiao, H. Dong, X. Zhang, Colorimetric-photothermal-magnetic three-in-one lateral flow immunoassay for two formats of biogenic amines sensitive and reliable quantification, Analytica Chimica Acta 1239 (2023) 340660.
[45] X. Li, D. Yu, H. Li, R. Sun, Z. Zhang, T. Zhao, G. Guo, J. Zeng, C.-Y. Wen, High-density Au nanoshells assembled onto Fe3O4 nanoclusters for integrated enrichment and photothermal/colorimetric dual-mode detection of SARS-CoV-2 nucleocapsid protein, Biosensors and Bioelectronics 241 (2023) 115688.
[46] S.C. Razo, V.G. Panferov, I.V. Safenkova, Y.A. Varitsev, A.V. Zherdev, B.B. Dzantiev, Double-enhanced lateral flow immunoassay for potato virus X based on a combination of magnetic and gold nanoparticles, Analytica Chimica Acta 1007 (2018) 50-60.
[47] S. Atta, M. Beetz, L. Fabris, Understanding the role of AgNO3 concentration and seed morphology in the achievement of tunable shape control in gold nanostars, Nanoscale 11(6) (2019) 2946-2958.
[48] J. Reguera, D. Jiménez de Aberasturi, N. Winckelmans, J. Langer, S. Bals, L.M. Liz-Marzán, Synthesis of Janus plasmonic–magnetic, star–sphere nanoparticles, and their application in SERS detection, Faraday Discussions 191(0) (2016) 47-59.
[49] H.M. Song, Q. Wei, Q.K. Ong, A. Wei, Plasmon-resonant nanoparticles and nanostars with magnetic cores: synthesis and magnetomotive imaging, ACS Nano 4(9) (2010) 5163-73.
[50] J. Li, P. Liang, T. Zhao, G. Guo, J. Zhu, C. Wen, J. Zeng, Colorimetric and Raman dual-mode lateral flow immunoassay detection of SARS-CoV-2 N protein antibody based on Ag nanoparticles with ultrathin Au shell assembled onto Fe3O4 nanoparticles, Analytical and Bioanalytical Chemistry 415(4) (2023) 545-554.
[51] A. Sharma, A.I.Y. Tok, P. Alagappan, B. Liedberg, Gold nanoparticle conjugated magnetic beads for extraction and nucleation based signal amplification in lateral flow assaying, Sensors and Actuators B: Chemical 312 (2020) 127959.